Few-Layer Antimonene by Liquid-Phase Exfoliation

Carlos Gibaja, David Rodriguez-San-Miguel, Pablo Ares, Julio Gómez-Herrero, Maria Varela, Roland Gillen, Janina Maultzsch, Frank Hauke, Andreas Hirsch, Gonzalo Abellán,* and Félix Zamora*

Abstract: We report on a fast and simple method to produce highly stable isopropanol/water (4:1) suspensions of few-layer antimonene by liquid-phase exfoliation of antimony crystals in a process that is assisted by sonication but does not require the addition of any surfactant. This straightforward method generates dispersions of few-layer antimonene suitable for on-surface isolation. Analysis by atomic force microscopy, scanning transmission electron microscopy, and electron energy loss spectroscopy confirmed the formation of high-quality few-layer antimonene nanosheets with large lateral dimensions. These nanolayers are extremely stable under ambient conditions. Their Raman signals are strongly thickness-dependent, which was rationalized by means of density functional theory calculations.

Currently, two-dimensional (2D) materials represent one of the most active research areas.[1] Apart from various well-stablished 2D materials, such as graphene, h-BN, and MoS$_2$, black phosphorus (BP) has received considerable attention over the last two years.[2] This is due to the fact that whereas graphene is a non-band-gap material and transition-metal dichalcogenides have a relatively large band gap for certain optoelectronic applications (1.5–2.5 eV),[3] the direct band gap of few- and single-layer BP is approximately 1.5 eV,[4] and this material therefore has appealing properties for electronic and ultrafast optoelectronic applications. However, isolated layers of BP are extremely sensitive to the surroundings, and strongly degrade upon air exposure, which limits their application.[2b] Thus the discovery of new 2D materials with

an appropriate band gap and stability under ambient conditions is a challenge of utmost importance.

Along this front, antimony is a good candidate as it is in the same group in the periodic table as phosphorus and exhibits an allotrope closely related to BP (Figure 1a). Indeed, theoretical calculations[5] have estimated the band gap for a single layer of antimony, or antimonene (we should point out that the name antimonene is not completely correct as there are no double bonds in its structure), to be about 1.2 eV. Antimonene has recently been isolated by mechanical exfoliation, and showed good stability under ambient conditions.[6] As for other 2D materials, micromechanical exfoliation provides high-quality flakes but is unsuitable for mass production. Liquid phase exfoliation (LPE) has been successfully applied to generate single- or few-layer (FL) samples of several 2D materials on large scale,[7] including stable suspensions of few-layer BP.[8]

Herein, we demonstrate that sonication of antimony crystals in a 4:1 isopropanol/water mixture without any surfactant produces a very stable suspension of micrometer-large FL antimonene over weeks, even under ambient conditions (see the Supporting Information for details). High-quality, few-layer antimonene nanosheets can thus be produced by liquid-phase exfoliation. Remarkably, the FL antimonene suspensions and the layers isolated on surfaces are very stable, even for weeks, under ambient conditions.

LPE of antimony crystals (see Figure 1a for their structure) was carried out by sonication of ground antimony crystals (see Figure 1b for a scanning electron microscopy

[*] C. Gibaja, D. Rodriguez-San-Miguel, Dr. F. Zamora
Departamento de Química Inorgánica
Universidad Autónoma de Madrid
28049 Madrid (Spain)
E-mail: felix.zamora@uam.es

D. Rodriguez-San-Miguel, Dr. F. Zamora
Instituto Madrileño de Estudios Avanzados en Nanociencia (IMDEA Nanociencia), Cantoblanco, 28049 Madrid (Spain)

P. Ares, Prof. J. Gómez-Herrero
Departamento de Física de la Materia Condensada
Universidad Autónoma de Madrid
28049 Madrid (Spain)

Prof. J. Gómez-Herrero, Dr. F. Zamora
Condensed Matter Physics Center (IFIMAC)
Universidad Autónoma de Madrid
28049 Madrid (Spain)

Dr. M. Varela
Facultad de CC. Físicas & Instituto Pluridisciplinar
Universidad Complutense de Madrid
28040 Madrid (Spain)

Dr. R. Gillen, Prof. J. Maultzsch
Institut für Festkörperphysik, Technische Universität Berlin
Hardenbergstrasse 36, 10623 Berlin (Germany)

Dr. F. Hauke, Prof. A. Hirsch, Dr. G. Abellán
Department of Chemistry and Pharmacy
University Erlangen-Nürnberg
Henkestrasse 42, 91054 Erlangen (Germany)
and
Institute of Advanced Materials and Processes (ZMP)
Dr.-Mack-Strasse 81, 90762 Fürth (Germany)
E-mail: gonzalo.abellan@fau.de

Supporting information for this article can be found under:
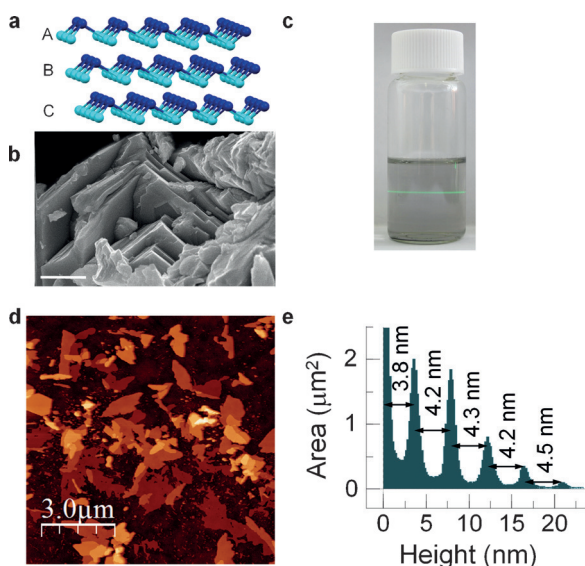http://dx.doi.org/10.1002/anie.201605298.

Figure 1. a) Structure of β-antimonene. b) SEM image of a layered antimony crystal (scale bar: 1 μm). c) Photograph of a dispersion of exfoliated FL antimonene showing the Faraday–Tyndall effect. d) Topographic AFM image of few-layer antimonene drop-casted onto SiO₂ showing flakes with micrometer lateral dimensions (scale bar: 3 μm). e) Height histogram of the image in (d) where the different thicknesses of the terraces can be readily seen. For the sake of clarity, the substrate peak has been cut to 2.5 μm². The constant minimum thickness of about 4 nm can be easily observed.

Figure 2. a) AFM topography showing several FL antimonene flakes with terraces of different heights. b) Height profile along the horizontal line of the image in (a) where the different thicknesses of the terraces can be readily seen. The minimum step height is about 4.0 nm. c) AFM image showing the atom periodicity. d) Fast Fourier transform (FFT) image taken from (c), showing the agreement with a hexagonal lattice as expected for β-antimony.

(SEM) image) in 4:1 *i*PrOH/water for 40 min at 400 W and 24 kHz, which yielded a colorless dispersion (Figure 1 c), showing the Faraday–Tyndall effect. Non-exfoliated material was removed by centrifugation at 3000 rpm (845 rcf) for 3 min to produce a stable dispersion with a concentration of about 1.74×10^{-3} g L^{-1}, as determined by atomic absorption spectroscopy (see the Supporting Information for a detailed analysis of the preparation conditions as well as information concerning solvent selection, optimization of the experimental exfoliation, centrifugation parameters, and UV/Vis spectroscopy).

Exfoliation of the antimony crystals was readily confirmed by atomic force microscopy (AFM). Figure 1 d shows a characteristic topographic image of FL antimonene flakes isolated on SiO₂ substrates (see the Supporting Information, Figure S6 for more AFM images). As reflected in the height histogram of the image (Figure 1 e), the step heights are multiples of about 4 nm. Furthermore, the flakes do not show the typical terrace characteristics of layered materials but well-defined structures with all heights being multiples of about 4 nm (Figures 1 d, e, 2 b, and S7). As it is well-known that the apparent AFM heights of layers obtained by LPE can be overestimated because of residual solvent[8, 9] as well as contributions from effects such as capillary and adhesion forces,[10] it seems likely that the apparent mono/bilayer thickness is about 4 nm. The overall lateral dimensions of the isolated nanosheets are greater than 1–3 μm² (see Figure S4 for a statistical analysis). Transmission electron microscopy (TEM) measurements further confirmed the success of the exfoliation (Figure S11).
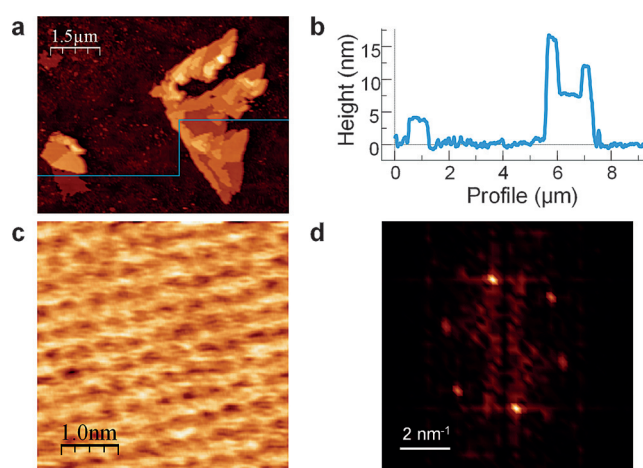
A high-resolution AFM topographic image taken of the lowest terrace (ca. 4 nm) of the isolated flake shown in Figure 2 a exhibits an atomic periodicity in line with that expected for β-antimony (Figure 2 c). To obtain insight into the stability of the nanosheets, atomic periodicity images were taken after exposing the flake to atmospheric conditions for more than two weeks, which confirmed the outstanding stability of few-layer antimonene under these ambient conditions (Figure S8).

Moreover, the Fourier transforms obtained from the AFM topographic images revealed hexagonal symmetry as expected for β-antimony, indicating excellent crystal quality. This finding is consistent with the results of other real-space techniques with atomic resolution (Figure S11). Aberration-corrected scanning transmission electron microscopy (STEM) combined with electron energy loss spectroscopy (EELS) was used to investigate the local structure and chemistry of the flakes. Figure 3 a shows a low-magnification high angle annular dark field (HAADF) image of a flake (top left) along with an atomic-resolution image of the crystal structure, both obtained at an acceleration voltage of 80 kV to prevent beam-induced damage. This structure (Figure 3 a) agrees with that of β-antimony along the [0 –1 2] direction. The samples were crystalline, and no major defects were observed. Compositional maps were obtained from the EEL spectra including the C K, Ca L$_{2,3}$, O K, and Sb M$_{4,5}$ absorption edges. Whereas little chemical inhomogeneity was detected within the flakes, the flake ends appeared to be somewhat damaged. A series of such maps from areas near the edges are shown in Figures 3 b and S8. Whereas a homogeneously distributed Sb signal was observed, a significant C signal was present within a few nanometers of the sample edge, pointing to some degree of surface contamination. Similarly, traces of O and Ca were detected within tens of nanometers from the edges, which is very likely due to the same reason (Ca is present because of solvent contamination).
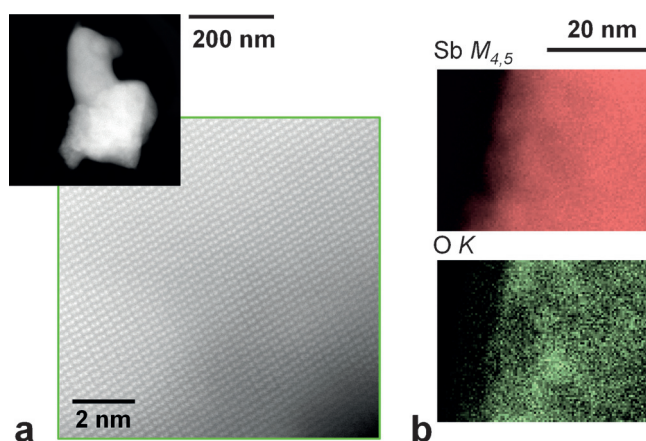
Figure 3. a) Low-magnification HAADF image of a flake (top left) along with an atomic-resolution image (image taken along the [0 −1 2] direction). b) Two-dimensional EELS maps acquired near the edge of the flake, showing the signals below the Sb M$_{4,5}$ (red) and O K (green) absorption edges.

Raman spectroscopy is a powerful method commonly used for the characterization of 2D materials. The Raman spectrum of bulk antimony when excited off resonance ($\lambda =$ 532 nm) exhibits two main phonon peaks (the A$_{1g}$ mode at 149.8 cm^{-1} and E$_g$ mode at 110 cm^{-1}).[11] Correlation of AFM and statistical Raman microscopy (SRM)[12] in a polydisperse sample revealed that flakes with an apparent thickness below about 70 nm (ca. 17 layers) hardly show any measurable Raman signal (Figure 4b). This unexpected dependence of the Raman intensity on the flake thickness is similar to that previously observed for micromechanically exfoliated flakes of antimony and analogous to what has been reported for mica nanosheets.[6, 13] Indeed, Figure 4b shows a series of single-point spectra measured at different positions, showing decreases in the peak intensities with a decrease in thickness. For comparison, we studied the influence of the laser excitation wavelength on a micromechanically exfoliated flake with a size of about 5.5 μm and a thickness of 10 nm, which had previously been analyzed by AFM, after its relocation in a Raman microscope by optical microscopy (see the Supporting Information and Figure S13 for additional information). As expected for this thickness, no Raman signal was detected, even after increasing the acquisition time and using different laser excitation wavelengths ($\lambda_{ex} = 785$, 633, 532, 473, 457, and 405 nm; Figure S11). However, the thinner flakes can be clearly located by SRM by monitoring the decrease in the silicon characteristic peak at about 521 cm^{-1} (Figure S15).

To complement our experimental results, we calculated the theoretical phonon spectra of bulk and few-layer antimony. We thus modeled the β-phase of bulk Sb, which consists of buckled quasi-2D layers of Sb in an ABC-type sequence (space group $\bar{R}3m$). For the primitive cell with rhombohedral axes and two atoms, this structure yields three optical modes, which are all Raman active: A pair of degenerate modes of E$_g$ symmetry, which corresponds to the in-plane transversal and longitudinal vibrations of the sublayers in opposite directions, gives rise to the experimentally observed Raman peak at
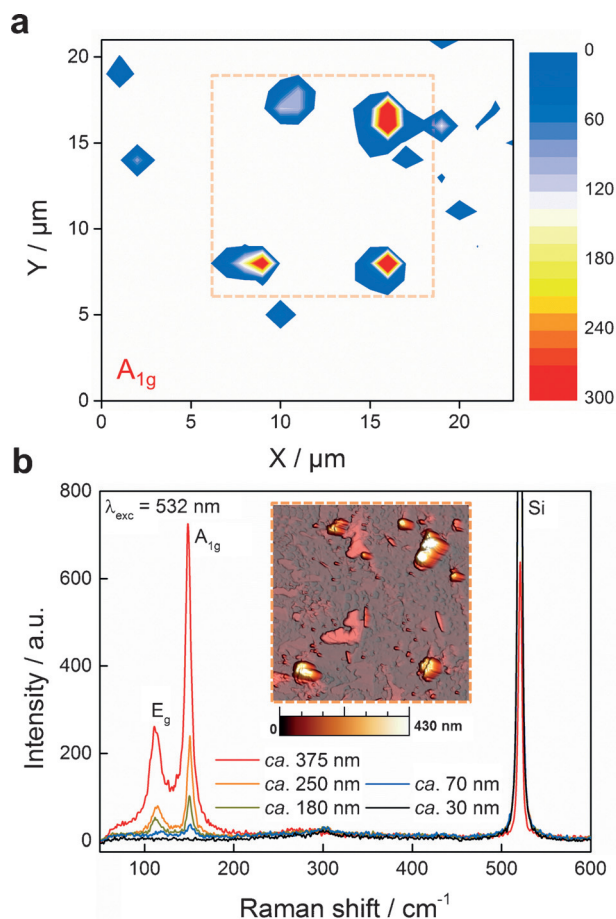

Figure 4. a) A$_{1g}$ intensity Raman mapping of solvent-exfoliated flakes deposited on a SiO$_2$/Si substrate, showing the presence of several flakes. b) Single-point spectra measured at different thicknesses according to the topographic AFM image (inset) of the same area studied in (a). The dashed square corresponds to the position of the AFM image shown in (b).

100 cm^{-1}. The peak at 150 cm^{-1} is caused by the third mode, opposite-in-phase out-of-plane vibrations of the sublayers of A$_{1g}$ symmetry. Our calculations underestimated both frequencies by about 9%, and we obtained values of 88 and 137 cm^{-1}. This softening of the optical phonons in DFT calculations has been observed before,[14] and appears to be related to the strong electron–lattice interaction and the negative Grüneisen parameter in antimony[11] and similar materials, such as bismuth.

For the few-layer system, our calculations predict a strong contraction of the in-plane lattice constant compared to the bulk material ($a = 4.3$ Å) when the film thickness is decreased to a trilayer ($a = 4.19$ Å), bilayer ($a = 4.15$ Å), and monolayer ($a = 4.01$ Å). As a result, the frequency of the bulk E$_g$ mode gradually increases from 88 to 167 cm^{-1} in monolayer Sb. In a similar fashion, the bulk A$_{1g}$ mode is blue-shifted with a decrease in film thickness, although to a smaller extent owing to the lower sensitivity of the out-of-plane modes to the in-plane lattice constant. In fact, the frequency increased from 137 cm^{-1} in the bulk to 208 cm^{-1} for the monolayer (1L) system. Interestingly, in the bilayer (2L) case, the frequencies of the E$_u$ and A$_{2u}$ modes are higher than those of the

corresponding E_g and A_{1g} modes. This seems counterintuitive as the sublayers oscillate in phase with their counterparts in the other layers for the E_u and A_{1g} modes (see the atomic displacement patterns in Figure 5). As a result, the intra-layer
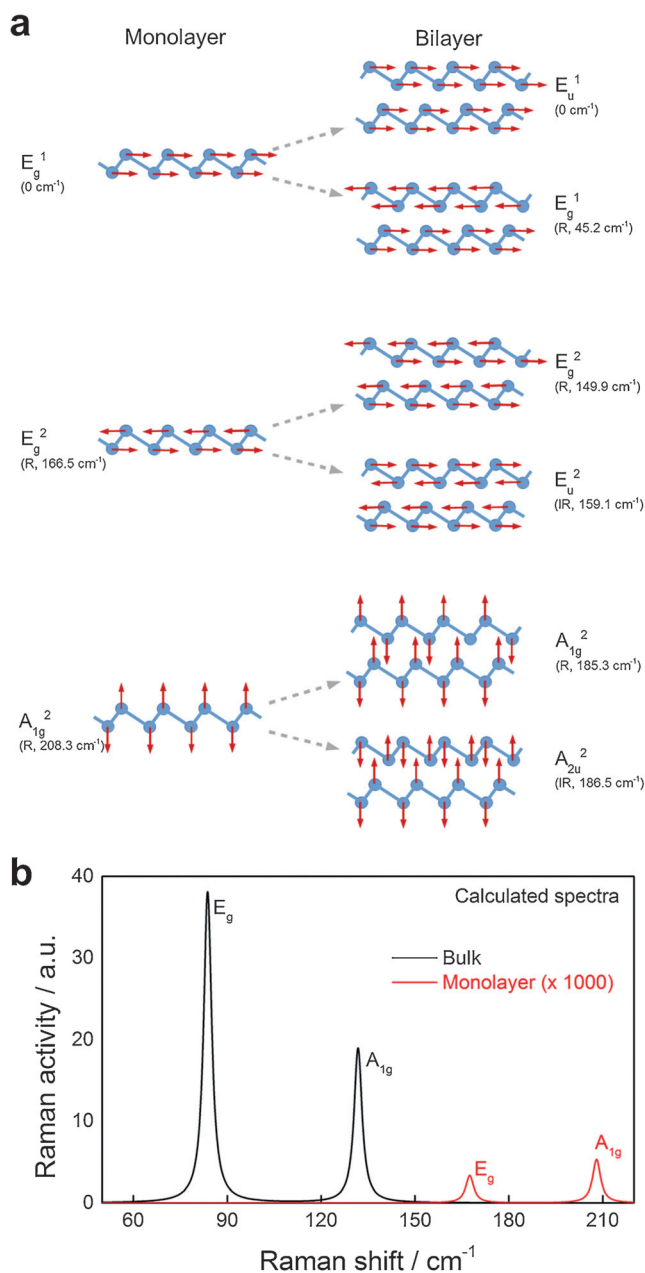

bond lengths do not change and should thus not contribute to the excitation energy of the vibration. However, it is possible that the Raman active E_g and A_{1g} modes benefit from energy compensation compared to the E_u and A_{2u} modes, for example, through strengthening of the weak covalent inter-layer bonds through periodic expansion and contraction. We observed a similar effect for the trilayer system.

We also calculated the non-resonant Raman intensities for the monolayer and bulk systems (Figure 5c).[15] Within the applied approximations, our calculations suggest a strong influence of the thickness on the simulated Raman activity, which decreases by about three orders of magnitude from bulk to monolayer Sb, which explains the experimentally observed absence of Raman signals in the thinnest flakes (Figure 4b). This behavior is in stark contrast to that of BN, for example, where the dependence of the predicted Raman tensor on the layer number is weak. It is thus possible that the experimentally observed suppression of Raman activity in Figure 4b for samples of sub-micrometer thickness has a contribution from a qualitative change in light–phonon coupling that is due to the decreasing layer number. We believe that this hypothesis warrants further investigation (see the Supporting Information for computational details and Tables with lattice constants and calculated frequencies).

The Raman results suggest that the isolated antimony nanosheets clearly consist of only few layers, as no Raman signal was observed for nanosheets with an AFM height of 30 nm. This implies that these nanosheets have a thickness of about 60 layers, assuming a theoretical thickness of about 0.5 nm for the antimony layers. In view of the theoretical calculations and experiments, it seems very unlikely to observe an impact on Raman spectra for nanosheets with a thickness over 60 layers. The Raman analysis therefore suggests that the apparent AFM thickness of about 4 nm could correspond to a single layer or bilayer of antimony.

In summary, we have reported on a procedure to generate very stable suspensions of high-quality single/few-layer anti-monene. Moreover, we have described the thickness-dependent Raman behavior of antimonene, defining the most important fingerprints for its Raman spectroscopic analysis. The scalable and environmentally friendly approach for isolating few-layer antimonene in aqueous solution will pave the way for the development of new antimonene-based technologies.

Figure 5. a) Atomic displacement patterns for the G point phonon modes in monolayer antimony (left) and the corresponding vibrations in the bilayer material (right). The E_g and E_u modes are doubly degenerate, and each mode has a partner mode (not shown) of the same frequency, with atoms vibrating perpendicularly to the plane of the paper. The out-of-plane acoustic A_{2u}^1 mode in monolayer Sb gives rise to two additional modes in the bilayer structure, the acoustic A_{2u}^1 and the optical A_{1g}^1 mode (both not shown). The calculated frequencies and Raman (R) or infrared (IR) activity are indicated in parentheses. b) Calculated Raman spectra for bulk antimony and single-layer antimonene. According to the experimental observations, the Raman signals for a monolayer are of very low intensity (>1000 times less Raman active than for the bulk counterpart), precluding its detection.

[1] a) Q. Tang, Z. Zhou, *Prog. Mater. Sci.* **2013**, *58*, 1244–1315; b) Q. Tang, Z. Zhou, Z. F. Chen, *Wires Comput. Mol. Sci.* **2015**, *5*, 360–379; c) R. Mas-Ballesté, C. Gomez-Navarro, J. Gomez-Herrero, F. Zamora, *Nanoscale* **2011**, *3*, 20–30; d) A. K. Geim, *Science* **2009**, *324*, 1530–1534; e) K. S. Novoselov, V. I. Fal'ko, L. Colombo, P. R. Gellert, M. G. Schwab, K. Kim, *Nature* **2012**, *490*, 192–200; f) A. C. Ferrari et al., *Nanoscale* **2015**, *7*, 4598–4810; g) M. Chhowalla, H. S. Shin, G. Eda, L. J. Li, K. P. Loh, H. Zhang, *Nat. Chem.* **2013**, *5*, 263–275; h) Q. Wang, D. O'Hare, *Chem. Rev.* **2012**, *112*, 4124–4155.

[2] a) A. Castellanos-Gomez, *J. Phys. Chem. Lett.* **2015**, *6*, 4873–4873; b) X. Ling, H. Wang, S. X. Huang, F. N. Xia, M. S. Dresselhaus, *Proc. Natl. Acad. Sci. USA* **2015**, *112*, 4523–4530.

[3] Q. H. Wang, K. Kalantar-Zadeh, A. Kis, J. N. Coleman, M. S. Strano, *Nat. Nanotechnol.* **2012**, *7*, 699–712.

[4] C. Tan, H. Zhang, *Chem. Soc. Rev.* **2015**, *44*, 2713–2731.

[5] a) S. Zhang, Z. Yan, Y. Li, Z. Chen, H. Zeng, *Angew. Chem. Int. Ed.* **2015**, *54*, 3112–3115; *Angew. Chem.* **2015**, *127*, 3155–3158; b) O. Ü. Aktürk, V. O. Özçelik, S. Ciraci, *Phys. Rev. B* **2015**, *91*, 235446.

[6] P. Ares, F. Aguilar-Galindo, D. Rodríguez-San-Miguel, D. A. Aldave, S. Díaz-Tendero, M. Alcamí, F. Martín, J. Gómez-Herrero, F. Zamora, *Adv. Mater.* **2016**, *28*, 6332–6336.

[7] a) V. Nicolosi, M. Chhowalla, M. G. Kanatzidis, M. S. Strano, J. N. Coleman, *Science* **2013**, *340*, 1226419; b) J. N. Coleman, *Acc. Chem. Res.* **2013**, *46*, 14–22.

[8] D. Hanlon, C. Backes, E. Doherty, C. S. Cucinotta, N. C. Berner, C. Boland, K. Lee, A. Harvey, P. Lynch, Z. Gholamvand, S. F. Zhang, K. P. Wang, G. Moynihan, A. Pokle, Q. M. Ramasse, N. McEvoy, W. J. Blau, J. Wang, G. Abellan, F. Hauke, A. Hirsch, S. Sanvito, D. D. O'Regan, G. S. Duesberg, V. Nicolosi, J. N. Coleman, *Nat. Commun.* **2015**, *6*, 8563.

[9] K. R. Paton, E. Varrla, C. Backes, R. J. Smith, U. Khan, A. O'Neill, C. Boland, M. Lotya, O. M. Istrate, P. King, T. Higgins, S. Barwich, P. May, P. Puczkarski, I. Ahmed, M. Moebius, H. Pettersson, E. Long, J. Coelho, S. E. O'Brien, E. K. McGuire, B. M. Sanchez, G. S. Duesberg, N. McEvoy, T. J. Pennycook, C. Downing, A. Crossley, V. Nicolosi, J. N. Coleman, *Nat. Mater.* **2014**, *13*, 624–630.

[10] P. Nemes-Incze, Z. Osvath, K. Kamaras, L. P. Biro, *Carbon* **2008**, *46*, 1435–1442.

[11] X. Wang, K. Kunc, I. Loa, U. Schwarz, K. Syassen, *Phys. Rev. B* **2006**, *74*, 134305.

[12] a) F. Hof, S. Bosch, J. M. Englert, F. Hauke, A. Hirsch, *Angew. Chem. Int. Ed.* **2012**, *51*, 11727–11730; *Angew. Chem.* **2012**, *124*, 11897–11900; b) J. M. Englert, P. Vecera, K. C. Knirsch, R. A. Schäfer, F. Hauke, A. Hirsch, *ACS Nano* **2013**, *7*, 5472–5482.

[13] A. Castellanos-Gomez, M. Wojtaszek, N. Tombros, N. Agrait, B. J. van Wees, G. Rubio-Bollinger, *Small* **2011**, *7*, 2491–2497.

[14] D. Campi, M. Bernasconi, G. Benedek, *Phys. Rev. B* **2012**, *86*, 075446.

[15] D. Porezag, M. R. Pederson, *Phys. Rev. B* **1996**, *54*, 7830–7836.